Am J Transl Res 2022;14(2):740-751
www.ajtr.org /ISSN:1943-8141/AJTR0140811

Original Article

A novel signal enhancement strategy for the detection of DNA oxidative damage biomarker 8-OHdG based on the synergy between β-CD-CuNCs and multi-walled carbon nanotubes

Ruoting Lin[1*], Shuang Zhou[2*], Huanan Zhao[4], Huasong Lin[1], Lixing Wang[2], Weipeng Hu[3], Hongzhi Gao[2,3], Bin Qiu[4]

[1]*Department of Neurology,* [2]*Clinical Center of Molecular Diagnosis and Therapy,* [3]*Department of Neurosurgery, Second Affiliated Hospital of Fujian Medical University, Quanzhou 362000, Fujian, China;* [4]*Ministry of Education Key Laboratory for Analytical Science of Food Safety and Biology, Fujian Provincial Key Laboratory of Analysis and Detection for Food Safety, Fuzhou University, Fuzhou 350108, Fujian, China.* [*]*Equal contributors.*

Received November 27, 2021; Accepted December 29, 2021; Epub February 15, 2022; Published February 28, 2022

Abstract: Objective: To propose a novel signal enhancement strategy based on the synergy between β-CD-CuNCs and multi-walled carbon nanotubes (MWCNTs) for the detection of DNA oxidative damage biomarker 8-Hydroxy-2'-deoxyguanosine (8-OHdG). Methods: The sensor was constructed with the β-CD-CuNCs-MWCNTs-nafion film and successfully used for the quantitative detection of 8-OhdG in the presence of biomolecules such as ascorbic acid (AA) and uric acid (UA). To investigate the surface morphology of the modified electrode, Transmission Electron Microscopy (TEM), Cyclic Voltammetry (CV) and Electrochemical Impedance Spectroscopy (EIS) were performed on bare and modified electrodes. Results: According to Differential Pulse Voltammetry (DPV) results, there was a linear relationship between peak current and concentration of 8-OhdG, ranging from 1.0×10^{-7} to 1.0×10^{-6} mol/L (R^2=0.9926) and 1.0×10^{-6} to 2.0×10^{-5} mol/L (R^2=0.9933). The detection limit (S/N=3) was 33 nmol/L. Conclusions: The proposed sensor had been successfully applied to the determination of 8-OHdG in human urine samples with high recovery rates.

Keywords: 8-Hydroxy-2'-deoxyguanosine, Carboxyl-multi-walled carbon nanotubes, β-CD-CuNCs, DNA oxidative damage, electrochemical biosensor

Introduction

In previous studies, researchers have reported that the normal metabolism of human cells and the activation metabolism of carcinogens may produce a large number of reactive oxygen species (ROS), including hydroxyl radicals (·OH), superoxide anion (O^{2-}), and hydrogen peroxide (H_2O_2) [1]. Reactive oxygen species play an important role in the occurrence, development and evolution of many chronic diseases. An appropriate amount of ROS is conducive to maintaining homeostasis, normal immune function and signal conduction in human body. However, excessive accumulation of ROS can affect structure and metabolism of nucleic acid, and lead to the damage of normal cells and tissues of human body and further causing various diseases [2, 3]. Studies have shown that ROS can lead to DNA oxidative damage, gene mutation, cell aging, and cancer. They are the pathogenic basis of some degenerative diseases related to age, such as tumor [4], diabetes [5], cardiovascular disease [6], Alzheimer's disease [7], and Parkinson's disease [8]. 8-OHdG was identified as an oxidative adduct formed by the binding of OH to the C-8 atom of guanine base under excessive ROS attack [9]. Kasai and Nishimura first reported the discovery of 8-OHdG in 1984 [10]. Since the formation and modification of 8-OHdG are not affected by diet and other factors, it is usually considered an effective index to measure oxidative stress and DNA oxidative damage.

Studies have shown that the content of 8-OHdG is closely related to the occurrence and development of tumors. Specifically, the level of 8-OHdG is highly expressed in humoral and cancerous tissues of patients with liver cancer [11], breast cancer [12], gastric cancer [13], and esophageal cancer [14]. Therefore, 8-OHdG is not only a key biomarker to evaluate the effects of endogenous oxidative damage in DNA, but also a factor in the initiation and development of carcinogenesis.

Recently, many methods for detecting 8-OHdG have been developed, including high-performance liquid chromatography with electrochemical detection (HPLC-ECD) [15], liquid chromatography-tandem mass spectrometry (LC-MS/MS) [16], enzyme-linked immunosorbent assay (ELISA) [17], capillary electrophoresis-electrochemistry detection method (CE-ECD) [18] and ^{32}P labeling [19]. In 2009, Miyachi et al. conducted in vitro selection of an aptamer by the Index Enrichment (SELEX) system [20]. Therefore, some efforts have been made to detect 8-OHdG based on aptamer and 8-OHdG specific binding. Liu et al. [21] constructed a simple and sensitive method for detecting 8-OHdG by using circular dichroism (CD). The aptamer is precisely matched with the complementary sequence modified with AuNPs to form a dimer, showing strong chiral behavior. After adding 8-OHdG, the high specific recognition and affinity between aptamer and 8-OHdG disrupted the dimeric structure, and the chiral signal was reduced, so 8-OHdG could be detected. Lv et al. [22] described a multi-mechanism-driven electrochemiluminescence (ECL) biosensor which uses competitive catalysis and steric hindrance effect to realize the quantitative detection of 8-OHdG by assembling hemin/G-quadruplex on carbon nitride nanosheets. The dynamic range of detectable concentrations from different mechanisms is integrated into a single sensor interface to more accurately control the detection sensitivity through competition between the two mechanisms. This may open up a new multi-channel biosensor for future methods. In conclusion, many contributions have been made to the detection of 8-OHdG. However, complex pre-processing steps, expensive instruments, and cumbersome operating procedures limit the applicability of these methods. In contrast, electrochemical methods of quantifying 8-OHdG based on the electrochemical oxidation activity of 8-OHdG show many advantages, such as high sensitivity, fast response and simple instrument operation. At the same time, electrochemical detection of 8-OHdG has been proven to be feasible because it undergoes an oxidation process through two-electron and two-proton charge transfer reaction [23]. The detection of 8-OHdG in a complex matrix (such as urine) has not met these requirements, so further research is needed.

With the rapid development of material science, carbon nanotubes (CNTs) have been applied in many different fields [24-26]. CNTs were first discovered by Japanese electron microscopist Iijima in 1991 [27]. The surface effect of CNTs and the existence of a large number of topological defects in the tube wall make the surface of CNTs substantially more reactive than other graphite variants. CNTs have become an important ideal material for the construct electrochemical biosensors because of their large aspect ratio, large specific surface area, and excellent physical, chemical and mechanical properties.

According to the number of layers of graphene sheets, CNTs can be divided into single-walled carbon nanotubes (SWCNTs) and multi-walled carbon nanotubes (MWCNTs). Specifically, SWCNTs are expensive and mainly used in field emission flat panel display [28]. In contrast, the MWCNTs are much cheaper while generally used to enhance the property of composite materials. When used as electrode materials, they could easily transfer electrons to other substances, showing better electron transfer characteristics. Sensors constructed from MWCNTs can detect the metal ions [29], amino acids [30], and miRNAs [31]. However, the tubes of MWCNTs have strong Van der Waals force and high aspect ratio. Because they are difficult to separate, they can easily be bound and entangled. In addition, they have low solubility in water and organic solvents and easily agglomerate. MWCNTs are difficult to disperse, which limits their application in many fields. Therefore, it is necessary to explore a new method to improve the dispersion and stability of MWCNTs.

In recently years, Metal nanoclusters (MNCs) have attracted extensive attention due to their unique electrical, physical, and optical properties. MNCs are composed of several to dozens of atoms [32]. The size of MNC is close to the Fermi wavelength of electrons. Due to its wave-

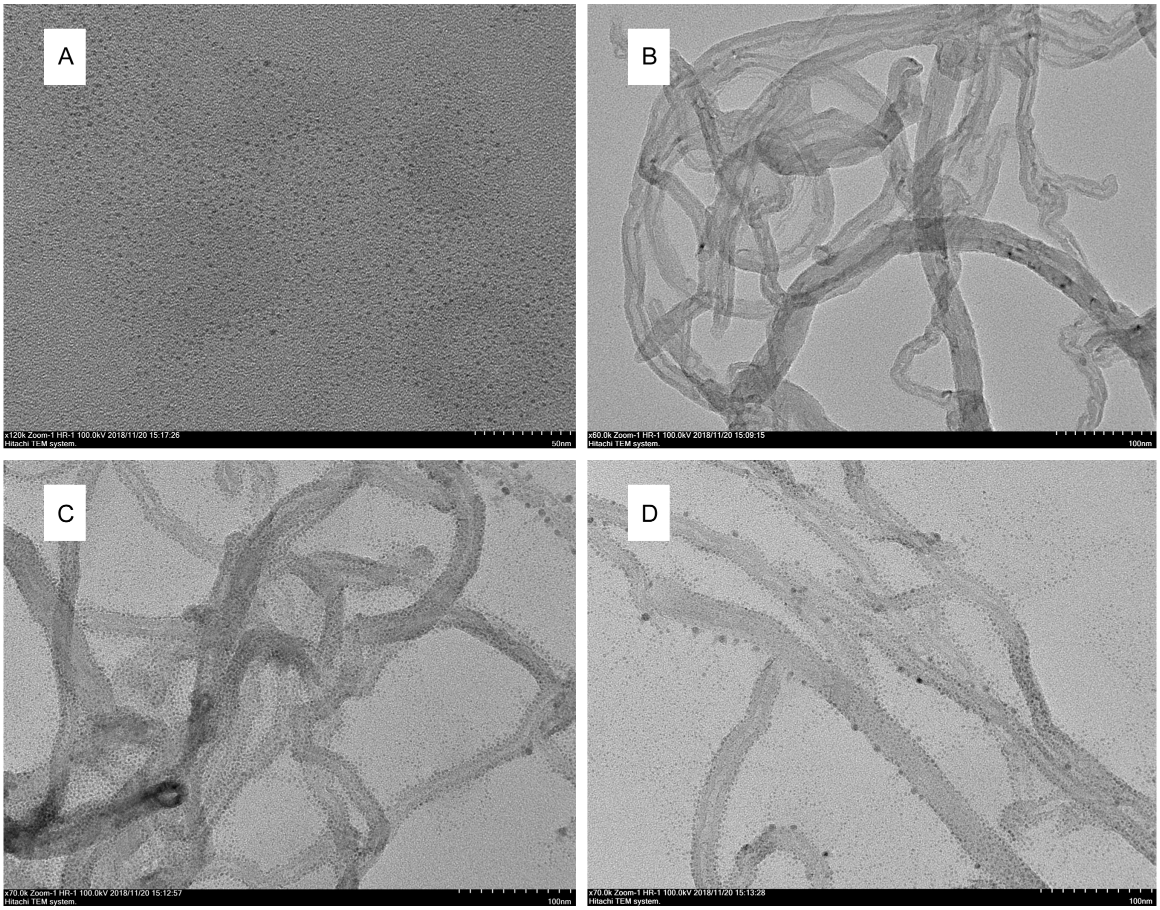

Figure 1. Transmission electron microscopy (TEM) of β-CD-CuNCs (A), MWCNTs (B) and β-CD-CuNCs-MWCNTs (C and D).

length between the metal atom and the nanoparticle, MNCs exhibit some special molecular characteristics, including discrete energy levels, size-dependent fluorescence, good photostability, and biocompatibility [33]. Based on its optical, electrochemical and catalytic properties, it has been successfully used to detect a variety of analytes, including metal ions [34, 35], anions [36], and biomolecules such as alkaline phosphatase ALP [37], miRNA [38], small molecule such as dopamine [39]. However, compared with the AuNCs and AgNCs, CuNCs are less reported and analyzed. Some related research is still in its early stages. Additionally, the preparation of CuNCs is relatively abundant, and they are cheap, and easy to obtain. Based on the above advantages, CuNCs are expected to be used in more fields in the future.

In this work, we proposed a novel electrochemical biosensor for the first time based on the synergistic effect of CuNCs and MWCNTs to construct a β-CD-CuNCs-MWCNTs-nafion film for the modified glassy carbon electrode (GCE). In the presence of ascorbic acid (AA) and uric acid (UA), a new signal amplification strategy was used to detect 8-OHdG. In addition, possible applications of the proposed sensor in the detection of these compounds in human urine samples were also investigated.

Experimental section

Preparation of β-CD-CuNCs

β-CD was used as a stabilizer, and $CuSO_4$ was reduced by AA to prepare β-CD-CuNCs. Briefly, 0.01125 g β-CD was dissolved in 3.0 mL of water. Then 400 μL of 10 mmol/L $CuSO_4$ and 100 μL of 1 mol/L AA were added to the β-CD solution. The mixture was heated and stirred at 40.0°C for 10 h to obtain pale yellow β-CD-CuNCs.

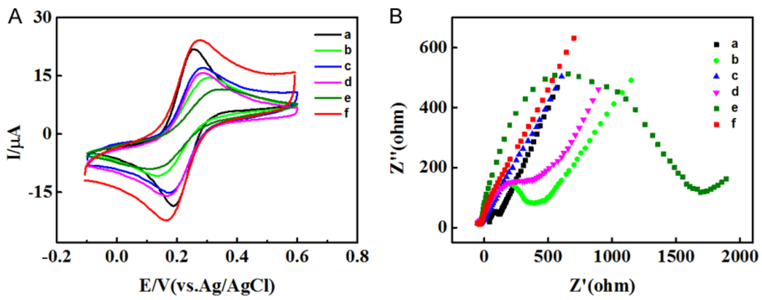

Figure 2. Cyclic Voltammetry (CV) (A) and Electrochemical Impedance Spectroscopy (EIS) (B) experiments on (a) bare glassy carbon electrode (GCE), (b) MWCNTs-nafion/GCE, (c) CuNCs-MWCNTs-nafion/GCE, (d) β-CD-MWCNTs-nafion/GCE, (e) β-CD-CuNCs-nafion/GCE and (f) β-CD-CuNCs-MWCNTs-nafion/GCE.

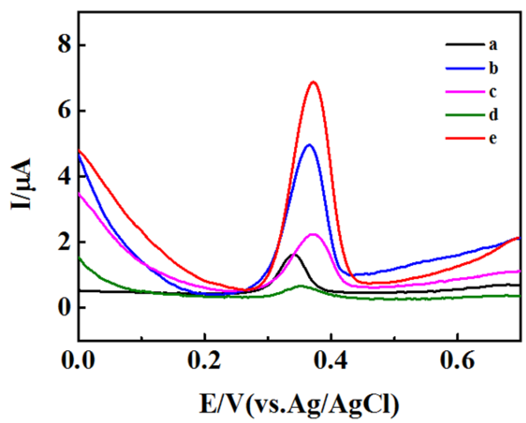

Figure 3. Differential Pulse Voltammetry (DPVs) on bare and modified electrodes in 0.1 mol/L PBS (pH=7.0) containing 10 μM 8-OHdG. (a) bare glassy carbon electrode (GCE), (b) MWCNTs-nafion/GCE, (c) β-CD-MWCNTs-nafion/GCE, (d) β-CD-CuNCs-nafion/GCE and (e) β-CD-CuNCs-MWCNTs-nafion/GCE.

Preparation of β-CD-CuNCs-MWCNTs-nafion suspension

0.65 mg of MWCNTs were dissolved in 1400 μL of water, stirred and sonicated for 30 min and 30 s, respectively. Then, 300 μL of β-CD-CuNCs was quickly added to the prepared MWCNTs suspension, stirred at room temperature for 6h to obtain a homogeneous β-CD-CuNCs-MWCNTs suspension. 20 μL of 0.50% nafion solution was added to 80 μL β-CD-CuNCs-MWCNTs suspension to obtain β-CD-CuNCs-MWCNTs-nafion suspension.

Preparation of modified electrodes

The glassy carbon electrode (GCE) was polished to a mirror surface with a 0.3 and 0.05 μm alumina slurry, rinsed with distilled water, and then it was ultrasounded in absolute ethanol and ultrapure water for 3 min, respectively, and dried under N_2.

7 μL of β-CD-CuNCs-MWCNTs-nafion suspension was dropped on the pretreated GCE surface and dried in the air. The obtained electrode was β-CD-CuNCs-MWCNTs-nafion/GCE. For further comparison, MWCNTs-nafion/GCE, β-CD-CuNCs-nafion/GCE, β-CD-MWCNTs-nafion/GCE were also prepared synchronously, and stored at 4°C for use.

Characterizations of modified electrodes

Transmission electron microscope (TEM, HT-7700, HITACHI, Japan) was used to characterize the composite materials.

Electrochemical measurements

The working electrode was placed in a test cell for electrochemical testing. CHI-660A Electrochemical Workstation (CH Instruments, USA) was used for electrochemical testing. Electrochemical characterization of bare and modified electrodes were performed by cyclic voltammetry (CV), electrochemical impedance spectroscopy (EIS) and differential pulse voltammetry (DPV). CV was performed in 0.1 mol/L KCl containing 1 mmol/L $[Fe(CN)_6]^{3-/4-}$ between -0.1 and 0.6 V at 50 mV/s. The EIS was performed in 0.1 mol/L KCl containing 5 mmol/L $[Fe(CN)_6]^{3-/4-}$. The DPV was performed in 0.1 mol/L PBS (pH=7.0) containing different concentrations of 8-OHdG, and the DPV parameters were chosen to obtain a pulse width of 0.05 s, an amplitude width of 5.0 mV and a quiet time of 2 s.

The three-electrode working system was selected for measurement: the β-CD-CuNCs-MWCNTs-nafion/GCE (d=3 mm) was the working electrode; the Ag/AgCl electrode was the reference electrode; and the platinum wire electrode was the counter electrode. 7 μL of β-CD-CuNCs-MWCNTs-nafion was dropped on the surface of the pretreated GCE and accumulated in a 0.1 mol/L pH 7.0 PBS containing different concentrations of 8-OHdG for 9 min to detect 8-OHdG.

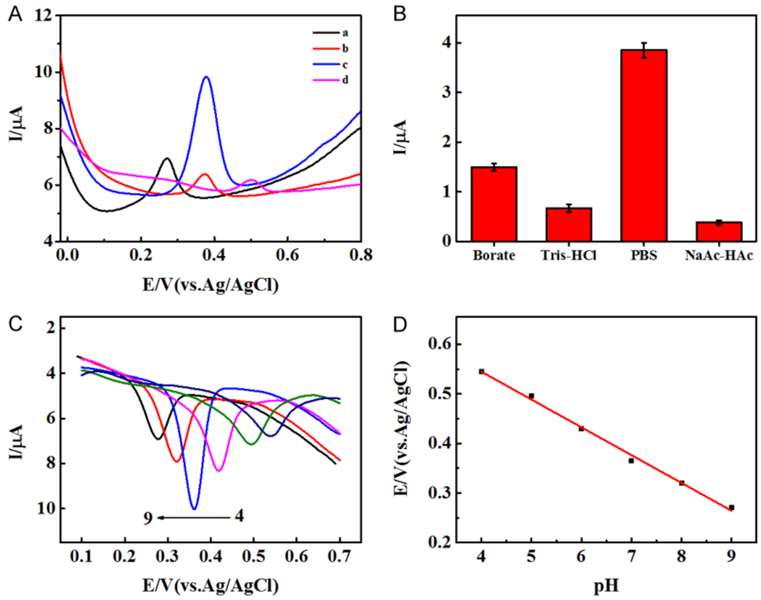

Figure 4. A and B. Dependence of the I_{pa} on different kinds of buffer solutions. C. Differential Pulse Voltammetry (DPVs) of 10 μM 8-OHdG on β-CD-CuNCs-MWCNTs-nafion/GCE in 0.1 mol/L PBS at different pH: 4.0, 5.0, 6.0, 7.0, 8.0, 9.0. D. The linear relationship of E_{pa} vs. pH.

Results

The morphology and structure of β-CD-CuNCs, MWCNTs, and β-CD-CuNCs-MWCNTs were characterized by transmission electron microscopy (TEM). As shows in **Figure 1A**, **1B**, the β-CD-CuNCs with an average size of 2-3 nm. The MWCNTs had diameter of 10-20 nm and length of 30 μm. **Figure 1C**, **1D** are β-CD-CuNCs-MWCNTs nanocomposites. It was clear that β-CD-CuNCs adhered to the surface of MWCNTs uniformly (See **Figure 1**).

CV and EIS experiments were performed to characterize modified electrodes and the results are shown in **Figure 2A**, **2B**. There are bare GCE (a), MWCNTs-nafion/GCE (b), (c) CuNCs-MWCNTs-nafion/GCE, (d) β-CD-MWCNTs-nafion/GCE, (e) β-CD-CuNCs-nafion/GCE and (f) β-CD-CuNCs-MWCNTs-nafion/GCE, respectively. Among them, the oxidation peak current on β-CD-CuNCs-MWCNTs-nafion/GCE was the highest, and the EIS was close to a straight line, indicating that its conductivity was the best.

Figure 3 shows the DPV of bare and modified electrodes in 0.1 M PBS containing 10 μM 8-OHdG. **Figure 4A**, **4B** show the DPV of 10 μM 8-OHdG in four different buffers including acetic acid-sodium acetate (pH=5.8), Tris-HCl (pH=7.0), borax buffer (pH=9.0) and PBS (pH=7.0). The influence of pH on the electrochemical behavior of 8-OHdG was investigated. The I_{pa} of the 8-OHdG in PBS was the highest, then PBS was selected as the system buffer in the following experiment. **Figure 4C** shows the effect of pH on the electrochemical behavior of 8-OHdG was further investigated over the range from pH 4.0 to 9.0 in 0.1 mol/L PBS. The I_{pa} increased first and then decreased. At pH=7.0, I_{pa} was the highest. Therefore, 0.1 M PBS (pH=7.0) was selected for the following experiments.

E_{pa}=0.7691-0.0561 pH (R^2=0.9946)

The effect of scan rate on the electrochemical behavior of 8-OHdG was researched, as shown in **Figure 5**. I_{pa} enhanced with the increase of scanning rate, which produced a good linear relationship, indicating that the oxidation of 8-OHdG on β-CD-CuNCs-MWCNTs-nafion/GCE was an adsorption control process [42].

$$E_{pa} = 0.3012 + 0.0234\, ln\, v\ (R^2 = 0.9919)\, E_{pa} = E^0 - \frac{RT}{(1-\alpha)nF} ln \frac{RTk^0}{(1-\alpha)nF} + \frac{RT}{(1-\alpha)nF} ln\, v$$

The ionic strength of electrolyte solution would affect the results of electrochemical measurements, so the concentration of the PBS was optimized. As shown in **Figure 6A**, with the concentration of PBS increasing, the peak current increased first and then decreased slightly. When the concentration of PBS was 0.1 mol/L, the peak current was the largest. Therefore, 0.1 mol/L PBS was used in the following experiment.

The volume of β-CD-CuNCs in the β-CD-CuNCs-MWCNTs suspension was optimized because the non-conductivity of β-CD might reduce the electrical conductivity of nanocomposite. As shown in **Figure 6B**, as the volume of β-CD-CuNCs increased, the I_{pa} value first increased and then decreased. The results show that the addition of 300 μL β-CD-CuNCs to synthesize

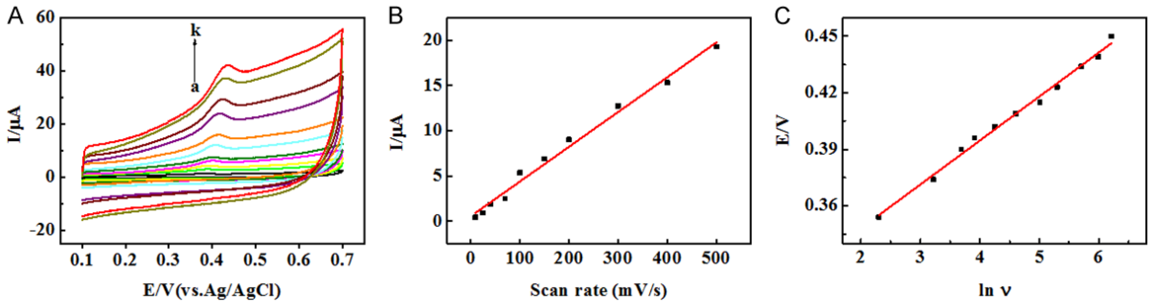

Figure 5. A. Cyclic Voltammetry (CVs) of 10 μM 8-OHdG on β-CD-CuNCs-MWCNTs-nafion/GCE with different scan rates (10-500 mV^{-1}) in 0.1 mol/L PBS (pH=7.0). B. The linear relationship of I_{pa} vs. v. C. The linear relationship of E_{pa} vs. ln v.

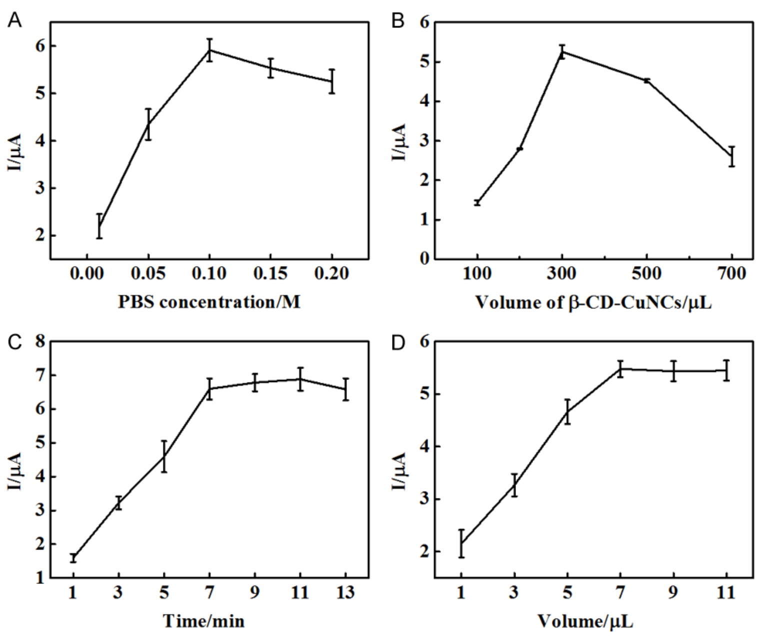

Figure 6. Dependence of I_{pa} on the concentration of PBS (A), the volume of β-CD-CuNCs (B), the accumulation time on β-CD-CuNCs-MWCNTs/GCE (C), the dropped volume of β-CD-CuNCs-MWCNTs-nafion on electrode (D).

β-CD-CuNCs-MWCNTs was the most suitable nanocomposite to the modified electrode.

Since the electrochemical process of 8-OHdG on the electrode surface was a process of adsorption control, the volume of the nanocomposite dropped on the electrode surface and the accumulation time in electrolyte solution were optimized separately. As shown in **Figure 6C**, I_{pa} increased with the increase of the volume of the coating. When 7 μL nanocomposite was dropped, I_{pa} no longer increased and reached a plateau, indicating that the adsorption of 8-OHdG on the electrode surface was saturated. Therefore, 7 μL was selected to be the most suitable coated volume. As shown in **Figure 6D**, I_{pa} gradually increased with the extension of the accumulation time, and after 7 min, the current value reached to the plateau. Therefore, 9 min was chosen as the most suitable accumulation time.

According to the above principles and optimized conditions, quantitative measurement of 8-OHdG by DPV were determined as shown in **Figure 7**. I_{pa} increased as the concentration of 8-OHdG increased in the range of 1.0×10^{-7}-1.0×10^{-6} mol/L and 1.0×10^{-6}-2.0×10^{-5} mol/L, and a good linear relationship was obtained. The linear regression equation was:

$$I_{pa}\ (\mu A)=0.069+0.662C\ (\mu M)\ R^2=0.9926 \quad (1)$$

$$I_{pa}\ (\mu A)=0.183+0.536C\ (\mu M)\ R^2=0.9933 \quad (2)$$

The detection limit was 33 nM, and the proposed sensor had a reasonable linear range and detection limit compared to other electrochemistry sensors in **Table 1**.

Since uric acid (UA) and ascorbic acid (AA) usually coexist with 8-OHdG in human metabolism, moreover, their electrochemical oxidation potentials are very close to 8-OHdG. It is necessary to check their interference on 8-OHdG detection. **Figure 8A** shows the DPV on

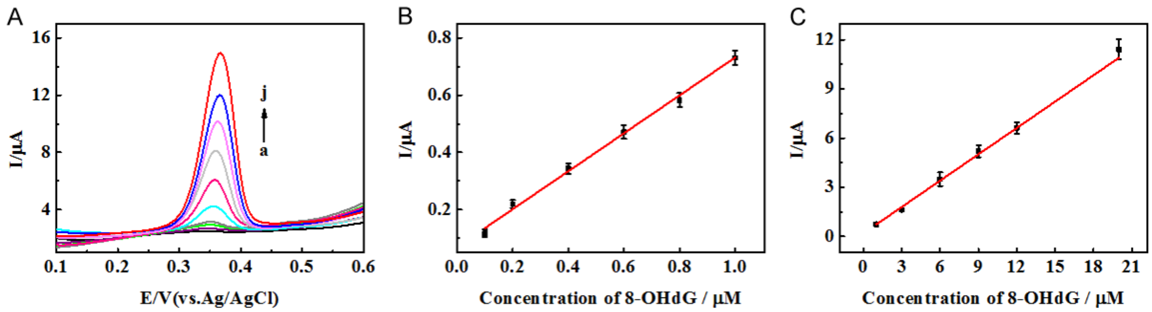

Figure 7. A. Differential Pulse Voltammetry (DPVs) of β-CD-CuNCs-MWCNTs-nafion/GCE with successive addition of 8-OHdG to 0.1 mol/L PBS (pH=7.0). B and C. are the calibration curve of E_{pa} vs. [8-OHdG].

Table 1. Comparison of various 8-OHdG sensors

Electrode	Linear range (μM)	Detection limit (μM)	Ref.
GCE/P-Arg/ErGO-AuNPs/GCE	0.001-10	0.001	M.Z.H. et al., 2018
ER-GO/Nafion/GCE	0.07-33.04	0.0012	Jia and Wang, 2013
PEI-MWCNTs/GCE	0.5-30	0.1	Gutiérrez et al., 2011
DNA-P3MT	0.28-4.2	0.056	Y. Wang et al., 2009
β-CD-CuNCs-MWCNTs-Nafion	0.1-20	0.033	this work

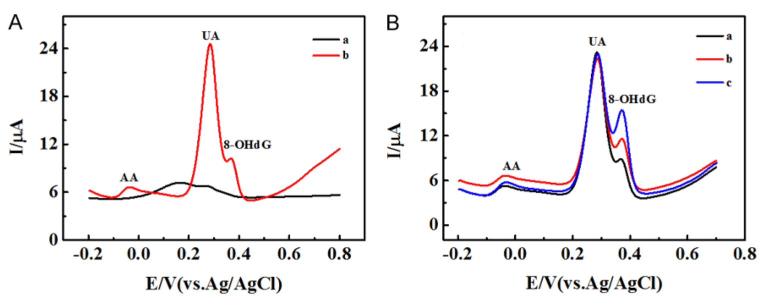

Figure 8. A. Differential Pulse Voltammetry (DPVs) on bare (a) and β-CD-CuNCs-MWCNTs-nafion/GCE in 0.1 mol/L PBS (pH=7.0) containing 3 μM 8-OHdG, 400 μM AA and 40 μM. B. DPVs of 8-OHdG (3, 5, 8 μM) on β-CD-CuNCs-MWCNTs-nafion/GCE in the presence of AA (400 μM) and UA (40 μM).

bare and β-CD-CuNCs-MWCNTs-nafion/GCE containing 3 μM 8-OHdG in the presence of 40 μM UA and 400 μM AA. Obviously, a bare electrode failed to separate the oxidation peaks among UA, AA and 8-OHdG, but the proposed 8-OHdG sensor did perfectly. **Figure 8B** shows three different and well-separated oxidation peaks at -0.032 V, 0.288 V and 0.376 V corresponding to the oxidation peaks of AA, UA, and 8-OHdG, respectively. Among them, the 8-OHdG oxidation peak current increased with concentration (3, 5, 8 μM) increasing, indicating that AA and UA had no effect on the detection of 8-OHdG. It was shown that β-CD-CuNCs-MWCNTs-nafion/GCE was promising for application for simultaneous detection of 8-OHdG, UA and AA.

The reproducibility experiment of five glassy carbon electrodes was estimated by comparing I_{pa} of 10 μM 8-OHdG. The relative standard deviation (RSD) was 3.44%. As shown in **Figure 9**, the β-CD-CuNCs-MWCNTs-nafion/GCE was placed in 1.0 mmol/L $[Fe(CN)_6]^{3-/4-}$ and 0.1 mol/L KCl, after 50 cycles of continuous cycle scanning at 50 mV/s, with the oxidation peak current still maintaining at 98.6% of the original response. The electrode was stored at 4°C for 4 weeks, and its current signal remained at the 96.0% of original. The above results show that β-CD-CuNCs-MWCNTs-nafion/GCE has good stability and reproducibility (See **Figure 9**). **Figure 10** shows the formation and electrochemical detection mechanism of 8-OHdG on β-CD-CuNCs-MWCNTs-nafion/GCE.

The 8-OHdG signal of DPV was not observed in the prepared samples. Therefore, the standard addition method was used, and the results are shown in **Table 2**. The recovery was between

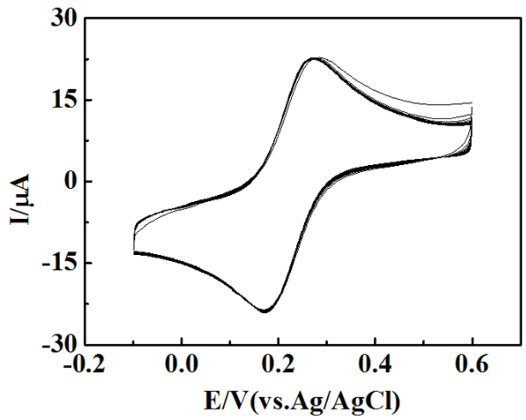

Figure 9. 100 segments continuous Cyclic Voltammetry (CV) scanning on β-CD-CuNCs-MWCNTs/GCE in 0.1 mol/L KCl containing 1.0 mmol/L $[Fe(CN)_6]^{3-/4-}$, at 50 mV/s.

97.4 to 101.3%, indicating that the proposed sensor could be used for the determination of 8-OHdG in real samples.

Discussion

Cyclic Voltammetry (CV) and Electrochemical Impedance Spectroscopy (EIS) were used to characterize the conductivity of different material modified electrodes, and Differential Pulse Voltammetry (DPV) was used to characterize the response of different material modified electrodes to 8-OHdG. The β-CD-CuNCs-c-MWCNTs/GCE modified electrode showed the best conductivity and the highest response signal to 8-OHdG.

β-CD-CuNCs, c-MWCNTs, and β-CD-CuNCs-c-MWCNTs composites were characterized by transmission electron microscopy (TEM). β-CD-CuNCs were uniformly attached to the surface of c-MWCNTs to improve the dispersion and stability of the composites. As far as we know, this is the first use of β-CD-CuNCs and c-MWCNTs to enhance the electronic conductivity and charge transfer in the electrochemical process of 8-OHdG, which amplifies the response signal of the target and improves the sensitivity.

The effects of pH and scanning rate on 8-OHdG were investigated and the β-CD-CuNCs-c-MWCNTs/GCE electrode surface on the electrochemical process was obtained. The mechanism of the electrochemical process on the surface of β-CD-CuNCs-c-MWCNTs/GCE electrode is double electron double proton transfer.

In addition, the oxidation peak potential shifts to a positive potential as the scan rate increases, and the linear regression equation between E_{pa} and the logarithm of scan rate (ln v) is:

$$E_{pa}=0.3012+0.0234\ ln\ v\ (R^2=0.9919) \qquad (3)$$

E_{pa} can be defined by the Lavilon equation [43]:

$$E_{pa} = E^0 - \frac{RT}{(1-\alpha)nF} ln \frac{RTk^0}{(1-\alpha)nF} + \frac{RT}{(1-\alpha)nF} ln\ v \qquad (4)$$

Where E^0 is the standard potential, k^0 is the standard heterogeneous reaction rate constant, α is the transfer coefficient, *n* is the number of transferred electrons, and v is scan rate. Therefore, *RT/(1-α) nF* was easily obtained from the slope of the above line. Typically, for an irreversible electrode process, α was taken as 0.5, so *n* was calculated to be 2. The number of electrons and protons in the electrochemical process of 8-OHdG were equal. Therefore, as shown in **Figure 11**, the electrochemical mechanism of 8-OHdG on β-CD-CuNCs-MWCNTs/GCE was a two-electron and two-proton process. The process was consistent with the previous work [23]. In addition, the oxidation peak potential (E_{pa}) shifted to lower potential as the pH increased. The reference indicated that the electrochemical process of 8-OHdG was related to the proton transfer process [40]. **Figure 4D** shows the linear regression equation of E_{pa} and pH was:

$$E_{pa}=0.7691-0.0561\ pH\ (R^2=0.9946) \qquad (5)$$

In the Nernst equation, from the linear relationship between potential and pH: -2.303 mRT/nF =-0.0561, where R is 8.314 $J \cdot mol^{-1} \cdot K^{-1}$, T is 298K and F is 96580 $C \cdot mol^{-1}$, and m/n was calculated as 0.95 close to 1, where m is the proton number and n is the number of transfer electrons, indicating that the number of protons and electrons were the same during the oxidation of 8-OHdG, which was consistent with previous work conclusions [41].

Study on the application of 8-OHdG in the electrochemical behavior of β-CD-CuNCs-c-MWCNTs/GCE electrode surface was at 1.0× 10^{-7} mol/L~1.0×10^{-6} mol/L and 1.0×10^{-6} mol/L~2.0×10^{-5} mol/L. The proposed sensor could detect 8-OHdG in the presence of AA and UA interference, and had good anti-interference, stability, and reproducibility. The detection of 8-OHdG in urine by labeling method provided a

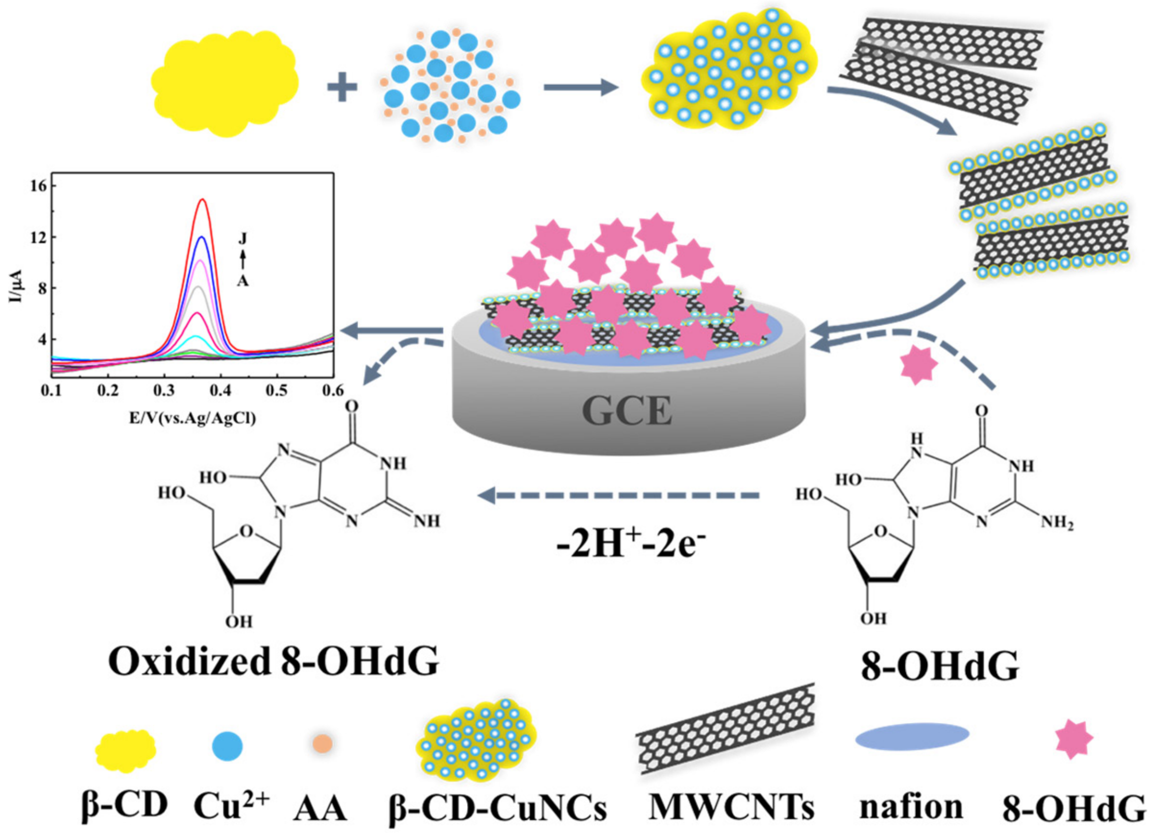

Figure 10. Electrochemical behavior and detection of 8-OHdG on β-CD-CuNCs-MWCNTs-nafion/GCE.

Table 2. Determination of 8-OHdG in human urine samples

Sample	Added (μM)	Found (μM)	Recovery %	RSD %
A	3.00	3.04	101.3	3.08
B	4.00	3.98	99.5	4.31
C	5.00	4.87	97.4	2.55

new way for electrochemical method to detect 8-OHdG.

Compared to the bare GCE, there was about a 3-fold enhancement in the peak current (I_{pa}) obtained on MWCNTs-nafion/GCE due to the good electrical conductivity and large surface area of the MWCNTs. β-CD-CuNCs did not respond well to the 8-OHdG yet. However, the stability on the electrode surface was excellent. After the combination of β-CD-CuNCs and MWCNTs, the stability was greatly improved and I_{pa} was also enhanced. This might be due to the uniform adherence of β-CD-CuNCs to the surface of MWCNTs, which better dispersed the MWCNTs and greatly improved the stability of the nanocomposite on the electrode. On the other hand, compared to MWCNTs, the β-CD-CuNCs-MWCNTs nanocomposite increased the electron conductivity and charge transport due to the synergy between β-CD-CuNCs and MWCNTs, which was beneficial to the electrochemical process of 8-OHdG on the electrode surface. This was the first time that the synergy of β-CD-CuNCs and MWCNTs reportedly enhanced the electrochemical oxidation process of 8-OHdG and improved the sensitivity.

Conclusion

8-OHdG is not only a key biomarker to evaluate the effects of endogenous oxidative damage in DNA, but also a factor of the initiation and development of carcinogenesis. Because of complex pre-processing steps, expensive instruments, and cumbersome operating procedures that limit the applicability of these methods, we proposed a novel signal enhancement strategy based on the synergy between β-CD-

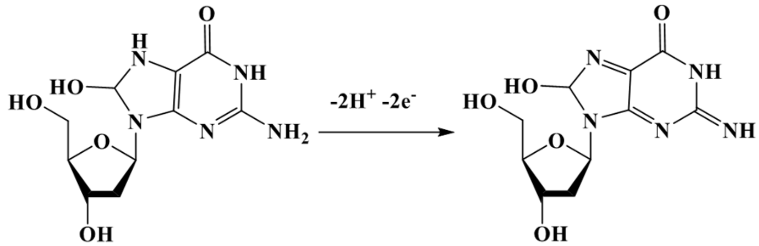

Figure 11. Schematics of the oxidation mechanism of 8-OHdG on β-CD-CuNCs-MWCNTs-nafion/GCE.

CuNCs and MWCNTs for the detection of DNA oxidative damage marker 8-OHdG. On the one hand, the good electrical conductivity and the large surface area of MWCNTs provided a carrier for the enrichment of 8-OHdG on the electrode surface, and β-CD-CuNCs was evenly distributed on MWCNTs, which better dispersed the MWCNTs. At the same time, the stability of the nanocomposite on the electrode was improved. On the other hand, based on the synergistic effect of the nanocomposite, electronic conductivity and charge transfer were enhanced, which was conducive to the electrochemical process of 8-OHdG on the electrode surface. In addition, the proposed β-CD-CuNCs-MWCNTs-nafion/GCE electrochemistry sensor successfully obtained the 8-OHdG signal in the presence of interference containing AA and UA, indicating that β-CD-CuNCs-MWCNTs-nafion/GCE have promising applications in the simultaneous detection of 8-OHdG, UA, and AA.

Acknowledgements

The authors gratefully acknowledge the financial support of the sailing fund project of Fujian Medical University (2017XQ1105), the Health and Education Joint Research Project of Fujian Province (2019-wj-13), and Sciences Funding (JT180195).

Disclosure of conflict of interest

None.

Address correspondence to: Hongzhi Gao, Clinical Center of Molecular Diagnosis and Therapy, Second Affiliated Hospital of Fujian Medical University, Quanzhou 362000, Fujian, China; Department of Neurosurgery, Second Affiliated Hospital of Fujian Medical University, No. 34 Zhongshan North Road, Quanzhou 362000, Fujian, China. Tel: +86-0595-2770061; E-mail: hongzhi_gao@hotmail.com; Weipeng Hu, Department of Neurosurgery, Second Affiliated Hospital of Fujian Medical University, No. 34 Zhongshan North Road, Quanzhou 362000, Fujian, China. Tel: +86-0595-2770061; E-mail: hwplcj@sina.com

References

[1] Shigenaga MK, Gimeno CJ and Ames BN. Urinary 8-hydroxy-2'-deoxyguanosine as a biological marker of in vivo oxidative DNA damage. Proc Natl Acad Sci U S A 1989; 86: 9697-9701.

[2] El-Kenawi A and Ruffell B. Inflammation, ROS, and mutagenesis. Cancer Cell 2017; 32: 727-729.

[3] Pendergrass W, Zitnik G, Tsai R and Wolf N. X-Ray induced cataract is preceded by LEC loss, and coincident with accumulation of cortical DNA, and ROS; similarities with age-related cataracts. Mol Vis 2010; 16: 1496-513.

[4] Priolli DG, Canelloi TP, Lopes CO, Valdivia JC, Martinez NP, Acari DP, Cardinalli IA and Ribeiro ML. Oxidative DNA damage and beta-catenin expression in colorectal cancer evolution. Int J Colorectal Dis 2013; 28: 713-722.

[5] Tatsch E, Bochi GV, Piva SJ, De Carvalho JA, Kober H, Torbitz VD, Duarte T, Signor C, Coelho AC, Duarte M, Montagner G, Da Cruz IB and Moresco RN. Association between DNA strand breakage and oxidative, inflammatory and endothelial biomarkers in type 2 diabetes. Mutat Res 2012; 732: 16-20.

[6] Shukla PC, Singh KK, Yanagawa B, Teoh H and Verma S. DNA damage repair and cardiovascular diseases. Can J Cardiol 2010; 26 Suppl A: 13A-16A.

[7] Kwiatkowski D, Czarny P, Toma M, Jurkowska N, Sliwinska A, Drzewoski J, Bachurska A, Szemraj J, Maes M, Berk M, Su KP, Galecki P and Sliwinski T. Associations between DNA damage, DNA base excision repair gene variability and Alzheimer's disease risk. Dement Geriatr Cogn Disord 2016; 41: 152-171.

[8] Petrozzi L, Lucetti C, Gambaccini G, Bernardini S, Del Dotto P, Migliore L, Scarpato R and Bonuccelli U. Cytogenetic analysis oxidative damage in lymphocytes of Parkinson's disease patients. Neurol Sci 2001; 22: 83-84.

[9] Floyd RA, West MS, Eneff KL, Hogsett WE and Tingey DT. Hydroxyl free radical mediated formation of 8-hydroxyguanine in isolated DNA. Arch Biochem Biophys 1988; 262: 266-272.

[10] Kasai H and Nishimura S. Hydroxylation of deoxyguanosine at the C-8 position by ascorbic acid and other reducing agents. Nucleic Acids Res 1984; 12: 2137-2145.

[11] Tang Y, Huang T and Wang J. Interaction between phenotypic oxidative DNA damage and polymorphism of DNA repair genes in a high-risk population of liver cancer. Tumor 2010; 30: 782-787.
[12] Himmetoglu S, Dincer Y, Ersoy YE, Bayraktar B, Celik V and Akcay T. DNA oxidation and antioxidant status in breast cancer. J Invest Med 2009; 57: 720-723.
[13] Wang YN, Zhao YF, Zhao Y, Luo XX, Guo ZJ and Zhang RX. Cancer risk associated single nucleotide polymorphisms of mitochondrial D-loop and 8-hydroxy-2'-deoxyguanosine levels in gastric cancer. Biotechnol Biotechnol Equip 2017; 31: 363-366.
[14] He HT, Zhao YF, Wang N, Zhang L and Wang CJ. 8-hydroxy-2'-deoxyguanosine expression predicts outcome of esophageal cancer. Ann Diagn Pathol 2014; 18: 326-328.
[15] Kawai K, Kasai H, Li YS, Kawasaki Y, Watanabe S, Ohta M, Honda T and Yamato H. Measurement of 8-hydroxyguanine as an oxidative stress biomarker in saliva by HPLC-ECD. Genes Environ 2018; 40: 5.
[16] Kurgan S, Onder C, Altingoz SM, Bagis N, Uyanik M, Serdar MA and Kantarci A. High sensitivity detection of salivary 8-hydroxy deoxyguanosine levels in patients with chronic periodontitis. J Periodontal Res 2015; 50: 766-774.
[17] Yin BY, Whyatt RM, Perera FP, Randall MC, Cooper TB and Santella RM. Determination of 8-hydroxydeoxyguanosine by an immunoaffinity chromatography-monoclonal antibody-based ELISA. Free Radic Biol Med 1995; 18: 1023-1032.
[18] Zhang SW, Zou CJ, Luo N, Weng QF, Cai LS, Wu CY and Xing J. Determination of urinary 8-hydroxy-2'-deoxyguanosine by capillary electrophoresis with molecularly imprinted monolith in-tube solid phase microextraction. Chin Chem Lett 2010; 21: 85-88.
[19] Mohamadkhani A, Moafi S, Fazli HR, Mirzaei S, Sharafkhah M, Besharat S, Montazeri G and Poustchi H. 8-hydroxy-2'-deoxyguanosin in peripheral leukocyte associated with HBsAg in patients with chronic hepatitis B. Jundishapur J Microbiol 2017; 10: e42609.
[20] Miyachi Y, Shimizu N, Ogino C, Fukuda H and Kondo A. Selection of a DNA aptamer that binds 8-OHdG using GMP-agarose. Bioorg Med Chem Lett 2009; 19: 3619-3622.
[21] Liu YJ, Wei M, Zhang LQ, Zhang YJ, Wei W, Yin LH, Pu YP and Liu SQ. Chiroplasmonic assemblies of gold nanoparticles for ultrasensitive detection of 8-hydroxy-2'-deoxyguanosine in human serum sample. Anal Chem 2016; 88: 6509-6514.
[22] Lv YQ, Chen SY, Shen YF, Ji JJ, Zhou Q, Liu SQ and Zhang YJ. Competitive multiple-mechanism-driven electrochemiluminescent detection of 8-hydroxy-2'-deoxyguanosine. J Am Chem Soc 2018; 140: 2801-2804.
[23] Guo ZP, Liu XH, Liu YL, Wu GF and Lu XQ. Constructing a novel 8-hydroxy-2'-deoxyguanosine electrochemical sensor and application in evaluating the oxidative damages of DNA and guanine. Biosens Bioelectron 2016; 86: 671-676.
[24] Salajegheh M, Ansari M, Foroghi MM and Kazemipour M. Computational design as a green approach for facile preparation of molecularly imprinted polyarginine-sodium alginate-multiwalled carbon nanotubes composite film on glassy carbon electrode for theophylline sensing. J Pharm Biomed Anal 2019; 162: 215-224.
[25] Zhang J, Guo XT, Zhou JP, Liu GZ and Zhang SY. Electrochemical preparation of surface molecularly imprinted poly(3-aminophenylboronic acid)/MWCNTs nanocomposite for sensitive sensing of epinephrine. Mater Sci Eng C Mater Biol Appl 2018; 91: 696-704.
[26] Tan K, Ma Q, Luo J, Xu S, Zhu Y, Wei W, Liu XY and Gu Y. Water-dispersible molecularly imprinted nanohybrids via co-assembly of carbon nanotubes with amphiphilic copolymer and photocrosslinking for highly sensitive and selective paracetamol detection. Biosens Bioelectron 2018; 117: 713-719.
[27] Iijima S. Helical microtubules of graphitic carbon. Nature 1991; 354: 56-58.
[28] Mukdasai S, Poosittisak S, Ngeontae W and Srijaranai S. A highly sensitive electrochemical determination of L-tryptophan in the presence of ascorbic acid and uric acid using in situ addition of tetrabutylammonium bromide on the beta-cyclodextrin incorporated multi-walled carbon nanotubes modified electrode. Sens Actuators B Chem 2018; 272: 518-525.
[29] Jiang M, Chen HR, Li SS, Liang R, Liu JH, Yang Y, Wu YJ, Yang M and Huang XJ. The selective capture of Pb2+ in rice phloem sap using glutathione-functionalized gold nanoparticles/multi-walled carbon nanotubes: enhancing anti-interference electrochemical detection. Environ Sci Nano 2018; 5: 2761-2771.
[30] Hashkavayi AB and Raoof JB. Ultrasensitive and reusable electrochemical aptasensor for detection of tryptophan using of Fe(bpy)(3) (p-CH3C6H4SO2)(2) as an electroactive indicator. J Pharm Biomed Anal 2019; 163: 180-187.
[31] Deng KQ, Liu XY, Li CX and Huang HW. Sensitive electrochemical sensing platform for microRNAs detection based on shortened multi-walled carbon nanotubes with high-loaded thionin. Biosens Bioelectron 2018; 117: 168-174.
[32] Hu X, Liu TT, Zhuang YX, Wang W, Li YY, Fan WH and Huang YM. Recent advances in the ana-

lytical applications of copper nanoclusters. Trac Trends Anal Chem 2016; 77: 66-75.
[33] Zhang LB and Wang EK. Metal nanoclusters: new fluorescent probes for sensors and bioimaging. Nano Today 2014; 9: 132-157.
[34] Ghosh SK, Rahman DS, Ali AL and Kalita A. Surface plasmon tunability and emission sensitivity of ultrasmall fluorescent copper nanoclusters. Plasmonics 2013; 8: 1457-1468.
[35] Goswami N, Giri A, Bootharaju MS, Xavier PL, Pradeep T and Pal SK. Copper quantum clusters in protein matrix: potential sensor of Pb2+ ion. Anal Chem 2011; 83: 9676-9680.
[36] Zhong YP, Wang QP, He Y, Ge YL and Song GW. A novel fluorescence and naked eye sensor for iodide in urine based on the iodide induced oxidative etching and aggregation of Cu nanoclusters. Sens Actuators B Chem 2015; 209: 147-153.
[37] Zhang LL, Zhao JJ, Duan M, Zhang H, Jiang JH and Yu RQ. Inhibition of dsDNA-templated copper nanoparticles by pyrophosphate as a label-free fluorescent strategy for alkaline phosphatase assay. Anal Chem 2013; 85: 3797-3801.
[38] Wang ZY, Si L, Bao JC and Dai ZH. A reusable microRNA sensor based on the electrocatalytic property of heteroduplex-templated copper nanoclusters. Chem Commun (Camb) 2015; 51: 6305-6307.
[39] Zou HY, Lan J and Huang CZ. Dopamine derived copper nanocrystals used as an efficient sensing, catalysis and antibacterial agent. Rsc Adv 2015; 5: 55832-55838.
[40] Jia LP, Liu JF and Wang HS. Electrochemical performance and detection of 8-hydroxy-2'-deoxyguanosine at single-stranded DNA functionalized graphene modified glassy carbon electrode. Biosens Bioelectron 2015; 67: 139-145.
[41] Langmaier J, Samec Z and Samcova E. Electrochemical oxidation of 8-oxo-2'-deoxyguanosine on glassy carbon, gold, platinum and tin(IV) oxide electrodes. Electroanalysis 2003; 15: 1555-1560.
[42] Yang LF, Wang B, Qi HL, Gao Q, Li CZ and Zhang CX. Highly sensitive electrochemical sensor for the determination of 8-hydroxy-2'-deoxyguanosine incorporating SWCNTs-Nafion composite film. J Sens 2015; 2015: 504869.
[43] Laviron E. General expression of the linear potential sweep voltammogram in the case of diffusionless electrochemical systems. J Electroanal Chem 1979; 101: 19-28.